Available online at www.sciencedirect.com
SCIENCE DIRECT
Journal of the European Ceramic Society 24 (2004) 969–974
ECERS
www.elsevier.com/locate/jeurceramsoc

Orientation selection in functional oxide thin films

G.J. Norga[a,b], L. Fé[a], F. Vasiliu[c,*], J. Fompeyrine[b], J.-P. Locquet[b], O. Van der Biest[d]

[a]IMEC, Kapeldreef 75, B-3001 Leuven, Belgium
[b]IBM Zurich Research Laboratory, Säumerstrasse 4, CH 8803 Rüschlikon, Switzerland
[c]National Institute of Materials Physics, PO Box MG-7, R-76900, Bucharest-Magurele, Romania
[d]KU Leuven, MTM Department, Kasteelpark 44, B-3001 Leuven, Belgium

Abstract

Mechanisms for orientation selection in complex oxide thin films are discussed, focusing on two examples: (1) development of a preferential texture in sol-gel prepared polycrystalline PZT films on Pt electrode layers and (2) selection of oxides for epitaxial growth on Si (111) and (100). In sol-gel PZT, a direct link was found between the formation of a well crystallized transient fluorite phase, promoted by reducing pyrolysis conditions, and the emergence of a strongly preferred (111) texture after crystallization. Meanwhile, in the MBE growth of epitaxial oxides on silicon, matching of silicon and oxide surface lattices is not a sufficient condition to achieve layer-by-layer growth, needed for planar films. In fact, for planar growth on Si(111), fluorite-structure compounds are required, while rocksalt and perovskite structure oxides are suited for the growth of low-roughness films on Si(100). These examples illustrate the important role played by surface energy in orientation selection.
© 2003 Elsevier Ltd. All rights reserved.

Keywords: Dielectric properties; Ferroelectric properties; Functional application; RZT; Sol-gel process

1. Introduction

Complex oxides are unparalleled by other materials classes in the diversity of their physical behavior, with properties spanning ferro-, pyro- and piezo-electricity, large dielectric constants, as well as high electro-optic figures of merit.[1] It has long been realized that integration of thin films of these so-called "functional" oxides with silicon could enable drastic improvements in speed and functionality of silicon-based microelectronics.

An example of "functional oxides microelectronics" which has already reached the marketplace is polycrystalline ferro-electric thin films grown on metallic electrode layers for use in nonvolatile memories (Ferro-Electric Random Access Memory = FERAM).[2] FERAM employs the natural bistability of ferroelectric oxides to store binary "1" and "0" in the polarization state of a ferroelectric capacitor. However, for optical applications of functional oxides, smooth, *single crystalline* films are indispensable, because of strong light scattering at grain boundaries and surface roughness.[3] Likewise, for electrical applications, a polycrystalline microstructure is undesirable as it puts limits on device downscaling.[‡] Therefore, single crystalline films are a necessary development to realize the full potential of functional oxides in microelectronics.

Both for single crystalline and polycrystalline films, the intrinsic crystalline anisotropy of functional oxides makes for a large dependence of film properties on film orientation. The development of methodologies for growing thin films (single crystal or polycrystalline) with a unique (or preferred) crystal orientation is therefore an important prerequisite for fully exploiting their properties in devices. In this paper we discuss the fundamental mechanisms controlling orientation selection in two selected systems: (1) polycrystalline PZT deposited by sol-gel on fiber-textured Pt (111) for application in FERAM; and (2) single-crystal, epitaxial oxide layers on silicon for use as high-k gate dielectric on silicon.

* Corresponding author.
E-mail address: fvasiliu@alpha1.infim.ro (F. Vasiliu).

‡ Lateral device dimensions are to remain large compared to the grain size of the films (typically about 200 nm), in order to avoid a large statistical spread in device behavior as device dimensions become comparable to the grain size.

0955-2219/$ - see front matter © 2003 Elsevier Ltd. All rights reserved.
doi:10.1016/S0955-2219(03)00405-9

2. Experimental

2.1. Sol-gel prepared PZT layers on Pt electrode layers

The Pt/Ti electrodes were prepared using RF sputtering deposition of 10 nm Ti followed by 100 nm Pt on thermally oxidized (100) Si wafers. The reactive Pt/Ti stack was subsequently stabilized by rapid thermal annealing (RTA) at 700 °C for 5 min in O_2. The resulting layers are columnar with a strong (111) fiber texture.

A PZT precursor solution with Zr/Ti ratio 30/70, prepared according to the procedure developed by Nouwen et al.,[4] was deposited by spin coating onto the preannealed Pt/Ti bottom electrodes. To compensate for Pb evaporation during thermal treatment, a Pb excess of 15% with respect to the stoichiometric amount was added. Three layers were deposited, resulting in a total film thickness of approximately 200 nm, with the pyrolysis step carried out after each layer on a temperature controlled hot plate. In our experiments, we studied the effect of varying pyrolysis temperature (between 350 and 450 °C), pyrolysis duration (10 s or 2 min), as well as the effect of a preliminary drying step at 200 °C. The crystallization treatment of the layers was always performed at 600 °C, 30 min on hot plate in air.

TEM, SAED and EDX investigations were performed by means of a Philips CM-30 electron microscope. Plan view and cross section specimens were prepared by the usual dimpling and ion milling techniques or by using FIB.

2.2. MBE growth of epitaxial oxides on silicon

For MBE growth of oxide layers on silicon, a chamber with a base vacuum of 5×10^{-10} mbar was employed. La and Zr were deposited by e-beam evaporation, Ba and Sr by evaporation from Knudsen cells. Oxygen partial pressure during growth varied from 2×10^{-8} to 2×10^{-7} mTorr while growth temperatures varied from 200 to 650 °C.

3. Results and discussion

3.1. Orientation selection in sol-gel derived PZT films on (111) textured Pt

A great variety of factors have been shown to affect orientation selection in sol-gel prepared PZT films. A factor that remains poorly understood, however, is the role of the pyrolysis conditions on texture development. As shown in Table 1, variations in the number, duration and temperature of pyrolysis steps have a large effect on film orientation after crystallization.[5] To elucidate the detailed structural cause behind such effects, we performed TEM-SAED studies on samples, pyrolysed under different conditions, varying pyrolysis temperature, duration and the number of pyrolysis steps. Shown in Table 1 are the pyrolysis conditions, orientation of the film after crystallization at 600 °C for 30 min. on hotplate, and a summary of the TEM-SAED findings.

While the existence of (111) and (100) orientation variants in PZT films has previously been attributed to the formation of interfacial template layers between PZT and Pt, our studies revealed instead a strong link between the existence of a well-crystallized pyrochlore phase in the as-pyrolysed films and the emergence of a preferential (111) orientation after the crystallization treatment. The presence of a well-crystallized pyrochlore phase was especially pronounced for low thermal budget pyrolysis (Film 4, pyrolysed for 10 s at 350 °C), as shown in the SAED pattern shown in Fig. 1. In contrast, higher pyrolysis temperatures and/or longer pyrolysis times result in essentially amorphous films, as for instance for sample 2 (XTEM image and SAED pattern shown in Fig. 2), which was pyrolysed for 2 min at 350 °C.

A closer study of several SAED patterns, collected in many well crystallized areas of film 4, yields a best fit to the metastable, oxygen deficient pyrochlore $Pb_2Ti_2O_{7-x}$, with a cubic structure (Fd3m space group) and lattice constant a = 10.5–10.6 Å. According to previous observations,[6–8] the systematic absence of any superlattice reflections, characteristic for the ordered pyrochlore structure, would indicate a metastable fluorite structure (disordered pyrochlore), with a unit cell which is only half that of the pyrochlore unit cell.

The formation of a well-crystallized intermediate fluorite phase is believed to be linked to the reduced oxygen partial pressure conditions caused by the burn-off of residual organics from the precursor.[5] This reduction in oxygen partial pressure is a transient effect, which is most pronounced during the initial stages of pyrolysis at moderate temperatures. This explains why the well-crystallized fluorite phase is most abundant in sample 4. Longer pyrolysis times and higher pyrolysis temperatures both result in higher oxygen partial pressure in the film. The quasi-amorphous structure of the pyrochlore in the sample pyrolysed for 2 min at 350 °C suggests that this higher oxygen potential destabilizes the fluorite structure. Evidently, under normal ambient oxygen partial pressure conditions, the disordered, oxygen deficient pyrochlore (i.e. fluorite structure $Pb_2(Zr, Ti)_2O_{7-x}$) is less stable than the ordered pyrochlore $Pb_2(Zr, Ti)_2O_7$. However, insufficient atom mobility due to the reduced temperatures during pyrolysis causes the fluorite structure PZT to transform to quasi-amorphous PZT rather than ordered pyrochlore. In Ref. 5, the greater degree of (100) orientation of the PZT after crystallization in film 2 was attributed to the fact that film 2 was found to contain large amounts of OH after

Table 1
Pyrolysis conditions, orientation after crystallization treatment and results of TEM analysis for selected samples

Sample	Drying step	Pyrolysis step	Orientation	Intermediate phase
1	No	2 min, 450 °C	(100) + weak (111)	Amorphous
2	No	2 min, 350 °C	(111)/(100) (mixed)	Amorphous
3	200 °C, 2 min	2 min, 350 °C	(111) + weak (100)	Nanocrystalline fluorite
4	No	10s, 350 °C	(111)	Nanocrystalline fluorite, well crystallized

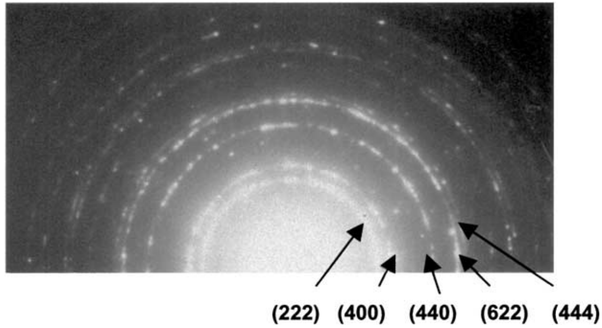

Fig. 1. Plan view SAED image of sample 4. Polycrystalline rings of $(Pb, Ti)_2O_6$ (indexing based on fluorite unit cell) are indicated.

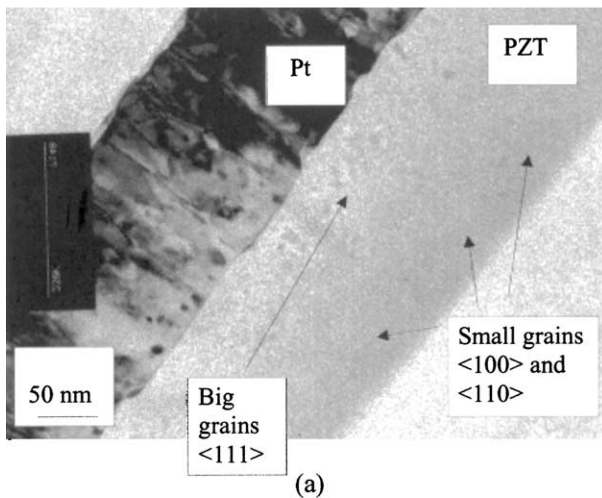

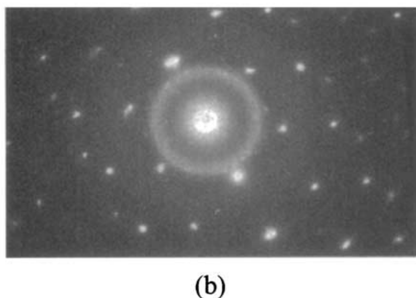

Fig. 2. (a) Plan view TEM image of sample 2; (b) corresponding SAED pattern. The spotty pattern is due to the Pt electrode layer.

pyrolysis, while film 3 was found to be OH-free after pyrolysis. These observations suggest that the absence of OH from film 3 may have facilitated the formation of a well-crystallized pyrochlore phase.

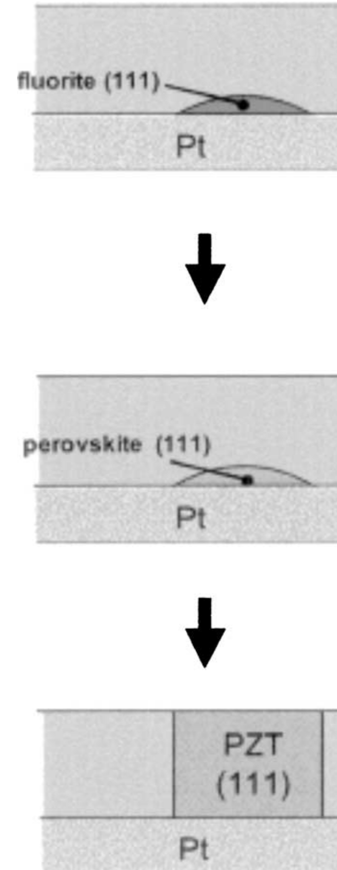

Fig. 3. Role of fluorite formation in texture selection of sol-gel PZT on Pt (111).

A possible explanation for the observed connection between intermediate pyrochlore phase crystallinity and preferred (111) orientation of the films is shown in Fig. 3. We speculate that the low surface energy of the (111) facets of fluorite structure may result in a preferential (111) orientation of the fluorite grains forming on top of Pt. Considering that several authors have identified the oxygen-deficient fluorite phase as a crucial intermediate for obtaining well crystallized perovskite at relatively low temperatures,[7,9,10] it seems reasonable to assume that the transformation of PZT–fluorite into PZT–perovskite occurs by reordering of the constituent atoms without any long-range diffusion. In fact, a simple model for the transformation of the fluorite into the perovskite structure (Fig. 4) can explain the transmission of the (111) fiber texture from fluorite to perovskite.[11]

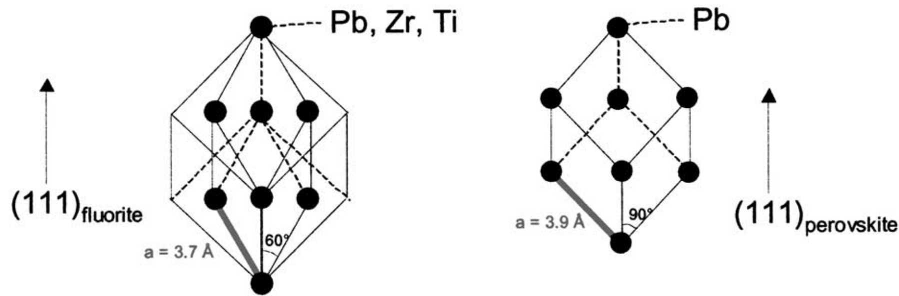

Fig. 4. Model for the transmission of (111) texture from fluorite to perovskite PZT.

3.2. MBE growth of high-ε gate dielectrics on silicon

The important role of surface thermodynamics in orientation selection in functional oxides can further be illustrated with an example from a rather different application area, namely the growth of epitaxial high-k oxides on silicon by MBE. Here, a key requirement is to obtain layer-by-layer growth conditions during film growth in order to ensure atomically smooth surfaces and interfaces. For growth to occur under layer-by-layer conditions, there are two important requirements: (1) low lattice mismatch between the oxide and silicon lattices, and (2) a low surface energy for the planes of the oxide film which are normal to the growth direction.

These two requirements dictate the choice of epitaxial oxides for growth on Si (100) and (111). To identify compounds satisfying the lattice matching requirement, the lattice constant vs temperature diagram shown in Fig. 5 can be used to establish the composition of different mixed oxides which are lattice-matched to silicon at a given temperature. Examples include the perovskite $(Ca_{.64}Sr_{.36})TiO_3$, the rocksalt structure oxide $(Ba_{.66}Sr_{.33})O$,* and the pyrochlore structure compound $(La, Zr)_2O_7$. Because of the second requirement, only those compounds for which the (100) crystal face has minimal surface energy, are suitable for growth on (100) Si. This explains why very smooth layers of lattice-matched, (100) oriented epitaxial perovskites and rocksalt structure oxides can be grown on silicon (100).[12–14] For instance, Fig. 6 shows the RHEED pattern obtained during growth of $(Ba_{.66}Sr_{.33})O$ on silicon (100). The streaky features indicate a smooth, two-dimensional growth process.

Meanwhile, the growth of $(La,Zr)_2O_7$ on $SrTiO_3$ (100) or Si (100) demonstrates clearly that lattice matching is not the sole requirement for obtaining planar growth of smooth, epitaxial films. In fact, deposition on (100) $SrTiO_3$ of lattice-matched $(La,Zr)_2O_7$ results in polycrystalline films. As illustrated in Fig. 7a, at a growth temperature of 650 °C the polycrystalline $(La,Zr)_2O_7$ on

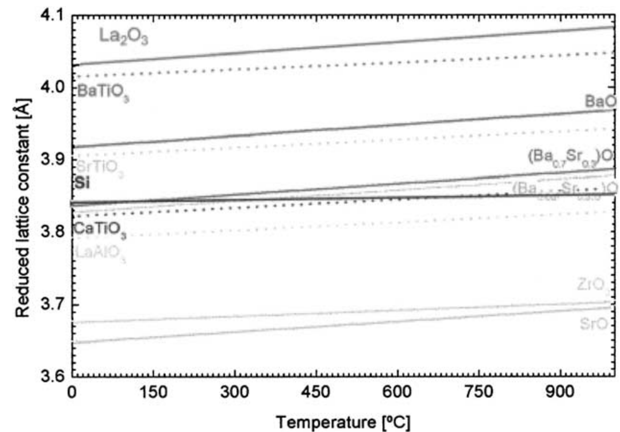

Fig. 5. Reduced lattice constant vs temperature in mixed oxide systems. For perovskite and rocksalt structure oxides the reduced lattice constant equals the real lattice constant. For silicon and $(La_2O_3)_x$ $(ZrO_2)_y$ mixed oxides the reduced lattice constant is a factor v2 smaller than the lattice constant of the cubic unit cell.

$SrTiO_3$ (100) is predominantly (111) oriented, demonstrating that nuclei select the orientation corresponding to their minimum surface energy. At higher growth temperatures ($T = 810$ °C, Fig. 7b), the texture becomes

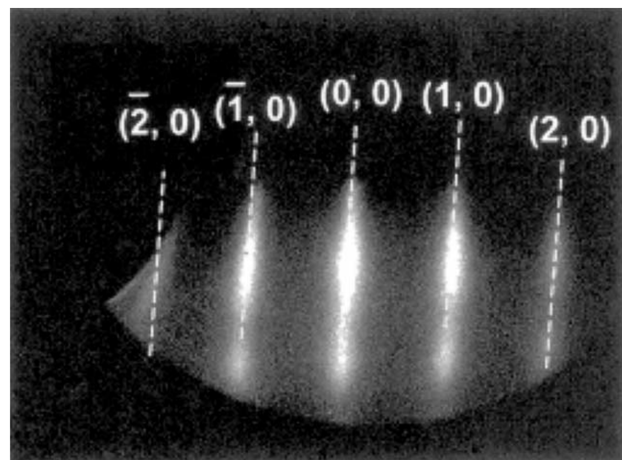

Fig. 6. RHEED pattern obtained during MBE growth of $(Ba_{.66}Sr_{.33})O$ on silicon (100). The sample is oriented along the Si <110> azimuth, corresponding to the <100> azimuth of $(Ba_{.66}Sr_{.33})O$. The streaks, indexed with reference to the $(Ba_{.66}Sr_{.33})O$ lattice, are indicative of smooth, two-dimensional film growth.

* The (100) silicon and (100) perovskite/rocksalt lattices can be matched by aligning $<100>_{Si}$ and $<110>_{oxide}$ and choosing a suitable binary composition of the perovskite.

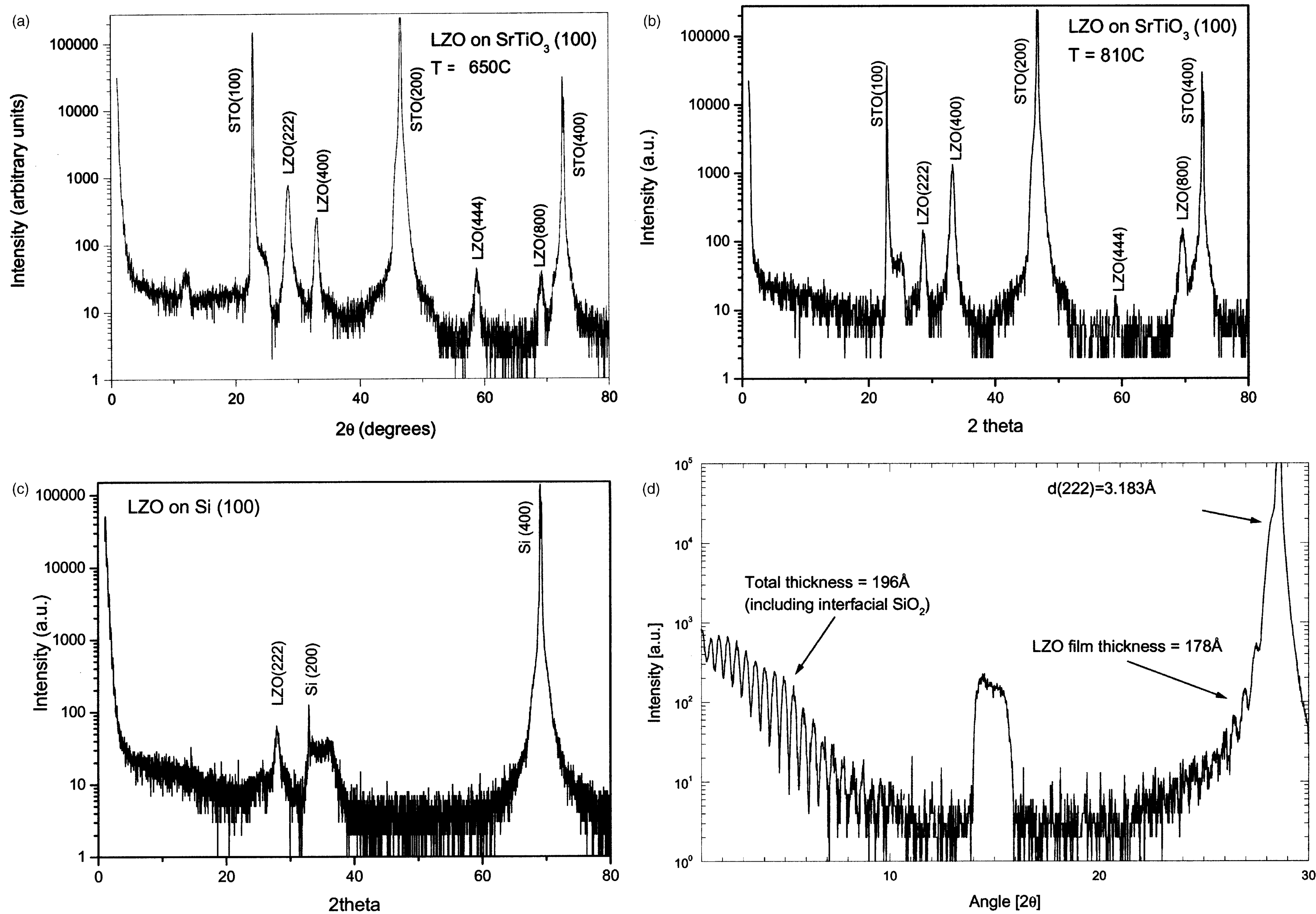

Fig. 7. (a) XRD pattern of $(La,Zr)_2O_7$ film, grown on $SrTiO_3$ (100) substrate at $T = 650$ °C, indicating a polycrystalline texture (preferentially (111) oriented). (b) XRD pattern of $(La,Zr)_2O_7$ film, grown on $SrTiO_3$ (100) substrate at high temperature ($T = 810$ °C), indicating a polycrystalline texture (preferentially (100) oriented). (c) XRD pattern of $(La,Zr)_2O_7$ film, grown on Si (100) substrate at $T = 650$ °C, indicating a polycrystalline texture (preferentially (111) oriented). The broad peak at $2\theta = 34$–36° is instrument-related. (d) XRD pattern of $(La,Zr)_2O_7$ film, grown on Si (111) substrate at $T = 650$ °C.

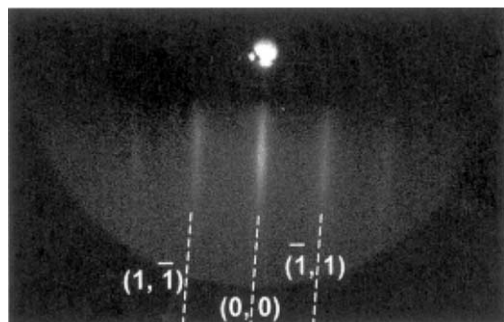

Fig. 8. RHEED pattern, taken along the Si <110> azimuth, obtained during MBE growth of $(La,Zr)_2O_7$ on silicon (111). The streaks are indicative of smooth, two-dimensional film growth.

predominantly (100), reflecting the tendency of the nuclei, as adatom mobility increases, to minimize their interfacial energy with the substrate by adopting the (100) orientation. However, the growth temperature of $(La,Zr)_2O_7$ on silicon is in practice limited to temperatures below 700 °C because at higher temperatures, silicide formation occurs.[14] Consequently, $(La,Zr)_2O_7$ films grown on silicon (100) at $T=650$ °C turn out polycrystalline with a (111) texture (Fig. 7c). In contrast, growth of $(La,Zr)_2O_7$ on Si(111) results in epitaxial (111) $(La,Zr)_2O_7$ layers, as reflected in the XRD spectrum shown in Fig. 7d. The thickness fringes, observed at low angle, indicate a total film thickness of 196 Å. Finite size intensity oscillations around the $(La,Zr)_2O_7$ (222) peak indicate a LZO film thickness of 178 Å. The position of the $(La,Zr)_2O_7$ (222) peak corresponds to a d-spacing of 3.183 Å. This value is 2% larger than the value for bulk $(La,Zr)_2O_7$, a result which is attributed to due to film off-stoichiometry. Finally, the streaky RHEED image obtained during growth of $(La,Zr)_2O_7$ on silicon (111) (Fig. 8) offers further evidence than an atomically smooth surface is maintained during the growth process.

4. Conclusions

In summary, oxygen-rich conditions during pyrolysis of sol-gel derived PZT films on Pt electrode layers result in a quasi-amorphous intermediate pyrochlore phase; while a reduced oxygen partial pressure in the film during pyrolysis cause a crystalline fluorite phase to nucleate homogeneously throughout the film. Fluorite grains forming on top of the Pt electrode are believed to be (111) textured because this orientation corresponds to the minimum surface energy crystal facets of the fluorite structure. Transformation of these grains to perovskite may explain (111) PZT texture observed after crystallization in the films, pyrolysed under reduced oxygen partial pressure conditions. In case the matrix from which the PZT nuclei form is amorphous, nuclei select the (100) orientation, corresponding to the minimum surface energy of the perovskite structure.

Secondly, analogies are drawn between orientation selection in PZT and the selection of oxides for epitaxial growth on silicon. To achieve planar growth, resulting in smooth films, firstly a film *composition* has to be chosen which corresponds to matching of the silicon and oxide lattices; and secondly, film *orientation* has to correspond to a minimum surface energy crystal plane. This twofold requirement is illustrated with two examples: growth of $(Ba_{.66}Sr_{.33})O$ on Si(100) and growth of $(La,Zr)_2O_7$ on Si (111).

Acknowledgements

While performing part of this work, G. J. N. was a postdoctoral fellow of the Fund for Scientific Research, Flanders (Belgium). The research reported here received partial support from the BWTS program of the Flemish Government and from the European Commission—IST Program (project "INVEST").

References

1. See for instance Moulson & Herbert, *"Electroceramics- Materials, Properties, Applications"*. Chapman & Hall, London, 1992.
2. Auciello, O., Scott, J. F. and Ramesh, R., *Physics Today*, 1998, **51**(7), 22.
3. Fork, D. K., Armani-Leplingard, F. and Kingston, J. J., *MRS Bulletin*, 1996, **July**, 53–58.
4. Nouwen, R., Mullens, J., Franco, D., Yperman, J. and Van Poucke, L. C., *Vibrational Spectroscopy*, 1996, **10**, 291.
5. Fé, L., Norga, G. J., Wouters, D. J., Maes, H. E. and Maes, G., *J. Mater. Res.*, 2001, **16**, 2499–2504.
6. Wilkinson, A. P., Speck, J. S., Cheetham, A. K., Natarajan, S. and Thomas, J. M., *Chem. Mater.*, 1994, **6**, 750.
7. Seifert, A., Lange, F. F. and Speck, J. S., *J. Am. Ceram. Soc.*, 1993, **76**, 443.
8. Lakeman, C. D. E., Xu, Z. and Payne, D. A., *J. Mater. Res.*, 1995, **10**, 2042.
9. Polli, A. D., Lange, F. F. and Levi, C. G., *J. Am. Ceram. Soc.*, 2000, **83**, 873.
10. Kim, J. H. and Lange, F. F., *J. Mater. Res.*, 1999, **14**, 1626.
11. Norga, G. J., Vasiliu, F., Fè, L., Wouters, D. and Van der Biest, O., *J. Mater. Res.*, 2003, **18**, 1232.
12. McKee, R. A., Walker, F. J. and Chisholm, M. F., *Phys. Rev. Lett.*, 1998, **81**(14), 3014.
13. Eisenbeiser, K., Finder, J. M., Yu, Z., Ramdani, J., Curless, J. A., Hallmark, J. A., Droopad, R., Ooms, W. J., Salem, L., Bradshaw, S. and Overgaard, C. D., *Appl. Phys. Lett.*, 2000, **76**(10), 1324.
14. Fompeyrine, J., Norga, G. J., Guiller, A., Marchiori, Ch., Locquet, J.-P., Siegwart, H., Halley, D. and Rossel, Ch., Proceedings of WODIM, the 12th Workshop on Dielectrics in Microelectronics, Grenoble, France, November 18–20, 2002. (Submitted for publication).